OPEN

Review article

Nuclear Medicine Communications

Management of respiratory motion in PET/computed tomography: the state of the art

Audrey Pépin[a], Joël Daouk[b], Pascal Bailly[a], Sébastien Hapdey[c,d] and Marc-Etienne Meyer[a,b]

Combined PET/computed tomography (CT) is of value in cancer diagnosis, follow-up, and treatment planning. For cancers located in the thorax or abdomen, the patient's breathing causes artifacts and errors in PET and CT images. Many different approaches for artifact avoidance or correction have been developed; most are based on gated acquisition and synchronization between the respiratory signal and PET acquisition. The respiratory signal is usually produced by an external sensor that tracks a physiological characteristic related to the patient's breathing. Respiratory gating is a compensation technique in which time or amplitude binning is used to exclude the motion in reconstructed PET images. Although this technique is performed in routine clinical practice, it fails to adequately correct for respiratory motion because each gate can mix several tissue positions. Researchers have suggested either selecting PET events from gated acquisitions or performing several PET acquisitions (corresponding to a breath-hold CT position). However, the PET acquisition time must be increased if adequate counting statistics are to be obtained in the different gates after binning. Hence, other researchers have assessed correction techniques that take account of all the counting statistics (without increasing the acquisition duration) and integrate motion information before, during, or after the reconstruction process. Here, we provide an overview of how motion is managed to overcome respiratory motion in PET/CT images. ***Nucl Med Commun*** **35:113–122 © 2014 Wolters Kluwer Health | Lippincott Williams & Wilkins.**

Nuclear Medicine Communications 2014, **35**:113–122

Keywords: compensation, correction, PET/computed tomography, respiratory motion, tracking

[a]Department of Nuclear Medicine, Amiens University Medical Centre, [b]Jules Verne University of Picardy, Amiens, [c]Nuclear Medicine Department, Henri Becquerel Center and Rouen University Hospital, Rouen and [d]QuantIF-LITIS laboratory, EA4108, University of Rouen, France

Correspondence to Pascal Bailly, MSc, Nuclear Medicine Department, Amiens University Medical Centre, Avenue René Laennec, F-80054 Amiens cedex, France
Tel: +33 322 455 964; fax: +33 322 456 011;
e-mail: bailly.pascal@chu-amiens.fr

Received 8 July 2013 **Revised** 11 October 2013 **Accepted** 21 October 2013

Introduction

PET imaging has proven value in cancer diagnosis, follow-up, and patient management [1,2]. It can also be used to design and adjust treatment plans in radiotherapy and chemotherapy [3].

The introduction of hybrid PET/computed tomography (CT) scanners over the last decade has improved the accuracy of attenuation correction and the ability to localize organs and tumors [4,5]. However, a number of physical and physiological phenomena can affect the accuracy of PET and CT images. Indeed, it has been shown that the diaphragm can move by as much as 20 mm in the craniocaudal axis [6] and that the liver can move by an average of 11 mm [7] during quiet breathing in the supine position. It is also well known that breathing induces rotational and/or translation movements in thoracic and abdominal organs to a varying extent [8–10]. For example, upper areas of the lungs are less subject to motion compared with the lower parts [6]. Moreover, Rodarte *et al.* [8] showed that even though the middle lobe of the canine lung and the lingula extend toward the diaphragm these structures are less subject to respiratory motion compared with the lower lobes.

CT images are acquired within a few seconds, whereas PET images are acquired over several minutes for each axial field of view. Even though the various CT slices in a free-breathing CT volume can be considered to be nonsynchronized 'snapshots', they will contain tissues from different respiratory states because the timeframe of a CT acquisition is roughly the same as that of the respiratory cycle (RC). Inversely, PET images of a moving uptake represent motion averaged over a few minutes. This difference in timeframe may induce registration errors, respiratory motion CT artifacts, and/or blurred PET images [11]. Furthermore, PET smearing effects and the attenuation correction derived from CT may in turn induce erroneous quantification of the standardized uptake value in PET.

Several procedures and devices have been developed with a view to avoiding these problems. Here, we review current methods for dealing with respiratory motion in PET/CT.

Respiratory motion tracking

Tracking techniques rely on an external device to estimate respiratory motion during PET/CT examinations. There is

0143-3636 © 2014 Wolters Kluwer Health | Lippincott Williams & Wilkins

DOI: 10.1097/MNM.0000000000000048

a proven correlation between respiratory motion and the displacement of internal organs [12–14]. Respiratory motion can be estimated by monitoring a physiological characteristic (such as the displacement of the thoracic cage or the volume of air exhaled) or a physical parameter (such as temperature or displacement of the skin surface). For analog sensors, the signal must be converted into a digital signal, which will be referred to as the respiratory signal (RS) throughout this review. Gated PET acquisition involves synchronization of the PET acquisition with the RS.

Signal measurement

Several solutions have been implemented on commercial imaging systems by the PET/CT device manufacturers, whereas academic researchers have assessed a number of other techniques.

The AZ-733V (Anzai Medical Corp., Tokyo, Japan) is a pressure sensor integrated into an elastic chest belt (Fig. 1a). The pressure sensor can thus detect the displacement of the abdominal wall as a function of pressure variations during the RC (i.e. low pressure during expiration and high pressure during inspiration). An analog-to-digital converter yields a signal that is recorded as a text file and can be used for offline processing [16].

Another widely used method involves the Real-Time Position Management (RPM) system (Varian Medical Systems, Palo Alto, California, USA). Two infrared reflective markers are placed on a plastic box positioned on the patient's thorax. A video camera placed at the end of the bed tracks the markers' motion during the RC (Fig. 1b). The markers' displacement is recorded by the video camera and yields an RS for further processing [16].

Otani *et al.* [18] compared the AZ-733V and RPM external respiratory tracking devices and found that the respective RSs were well correlated.

Sensors measuring air temperature changes during respiration can also be used. Indeed, the air temperature in the upper airways during inspiration is lower than that during expiration because the air is warmed during its passage through the lungs. A high time resolution is needed for this type of sensor. In one embodiment of this system, a high-sensitivity thermistor can be mounted inside a conventional oxygen mask. In another variant, a probe is placed close to the patient's nostrils (BioVet CT1 System; Spin Systems, Brisbane, Australia) (Fig. 1c) [16]. Boucher *et al.* [19] have demonstrated the clinical feasibility of this type of device. However, this tracking device has not yet been implemented on commercial PET scanners and has not been greatly characterized in the literature.

A spirometer can be used to estimate the volume of air inhaled or exhaled during breathing. It can be placed close to the patient's nostrils (PMM Spirometer; Siemens Medical Systems, Erlangen, Germany [16]) or mouth (CPX Spirometer; Medgraphics, St Paul, Minnesota, USA [17]) (Fig. 1d). However, use of this system with a clinical PET/CT gantry has not been investigated yet. The main drawbacks of this system are discomfort for the patient and the inability to provide simultaneous oxygen assistance. Similarly, Didierlaurent *et al.* [20] connected a pneumotachograph (which measures the change in lung volume over time via the exhaled respiratory flow) to a PET/CT gantry.

Synchronizing a respiratory signal with PET or computed tomography data

The RS can be synchronized with four-dimensional (4D) PET or CT data. In list-mode (LM) acquisitions, coincidence events and time tags are recorded in real time. As shown by Bruyant *et al.* [21], a tag can be stored within the LM file whenever the user-defined RS threshold is reached. Given that the LM retains time data, PET synchronization and processing can be performed after the acquisition.

Compensation techniques

The respiratory gating methods based on motion tracking mostly use LM PET data to take advantage of the temporal component. There are two ways to process respiratory-gated PET data: dividing the RS into multiple phases (in multiphase or multibin methods) or considering only a single phase (in single-bin methods).

Multibin methods

The RS can be processed as a function of time or amplitude. In both time-based and amplitude-based methods, the RC can be divided into equal-sized or different-sized bins. We shall detail each of these approaches in the following sections.

Time-based methods

In the time-based approach, each RC (as delimited by two gating tags in the LM) is divided into several bins [22–27]. Several different approaches have been suggested. Dawood *et al.* [28] set a fixed time for all bins and for all RCs (Fig. 2a). However, depending on the RC length, some PET data may be lost. Manufacturers have offered time-based, respiratory-gated PET processing based on the division of each RC into the same number of bins (Fig. 2b) [29]. In this method, users have to define a range of acceptable RC frequencies. Data from abnormally short or long RCs are excluded from the analysis.

The number of bins is an important determinant of image quality. In fact, there is a tradeoff between residual motion and counting statistics: the lower the number of bins, the weaker the blurring removal but the higher the signal-to-noise ratio in each bin. Conversely, a high

Fig. 1

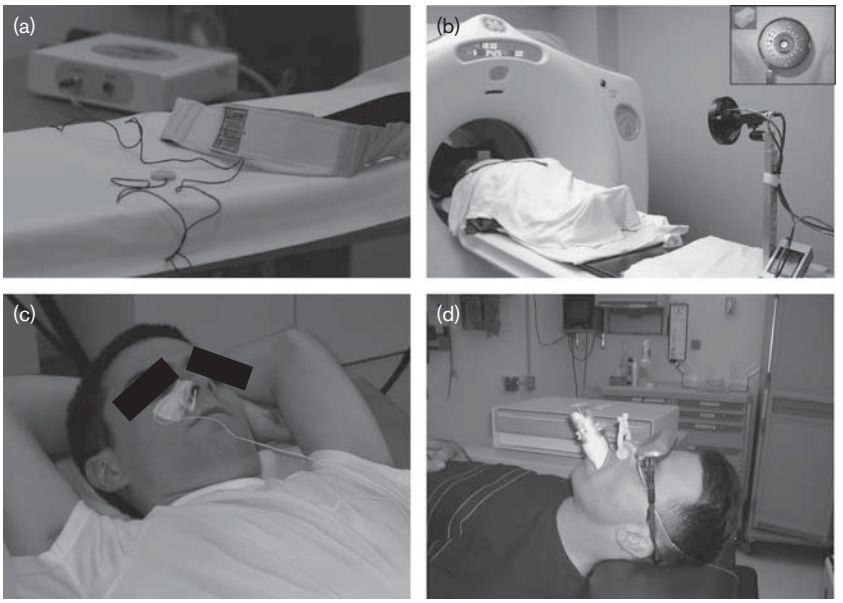

(a) The AZ-733V pressure belt (Anzai Medical Corp.). (b) The Real-Time Position Management (RPM) system (Varian Medical Systems) (reprinted with permission from AAPM and Dr Sadek Nehmeh [15]). Copyright AAPM, College Park, MD, USA. All permission requests for this image should be made to the copyright holder. (c) The BioVet CT1 System (Spin Systems) (reprinted with permission from Dr Axel Martinez-Möller [16]). Copyright Technical University Munich, Germany. All permission requests for this image should be made to the copyright holder. (d) The CPX Spirometer (Medgraphics) (reprinted with permission from AAPM and Dr Bhudatt Paliwal [17]). Copyright AAPM, College Park, MD, USA. All permission requests for this image should be made to the copyright holder.

number of bins translates into negligible residual motion and a marked decrease in the signal-to-noise ratio. On the basis of Monte Carlo methods, Vauclin *et al.* [30] suggested that, although the accuracy in lesion volume estimation increases with the number of bins considered, there is a corresponding decrease in overall lesion detectability because the total count statistic was divided by the number of gated bins. Dawood *et al.* [31] reported that six respiratory bins constituted the optimal tradeoff between residual motion in an individual bin on one hand and image quality on the other.

Furthermore, the degree of motion compensation differs from one bin to another. This is due to differences in tissue velocity in the different phases of the RC; some bins correspond to a very steep part of the RS, where the tissue velocity is high. Next, uptake restitution of the moving target is flawed by high residual motion. Moreover, respiratory amplitude varies significantly from one individual to another. Hence, events from different tissue positions may become mixed within a single bin, leading to a blurred image of the target. To minimize these differences and regularize the RC, some systems offer 'vocal coaching'. This method is only partially effective, as 'coached' respiration is not always regular [15,32].

Many researchers have compared gated PET images with ungated PET images (i.e. those acquired in the absence of RC synchronization) [22–27]. Table 1 summarizes the results associated with time-based methods [24–27]. Depending on the lesion size, respiratory motion can lead to major errors in uptake detection. For motionless lesions, the detection limit is roughly two or three times the tomograph's spatial resolution [33]. The quantification bias increases as the lesion's largest axis decreases [34]. Adding a motion component raises the limit of detection and increases quantification bias.

The time-based approach has been implemented by all manufacturers because it does not require access to the RS. Indeed, the RS is generally obtained by third-party devices and is neither available nor processed on reconstruction workstations.

Amplitude-based methods

In this approach, the RS is divided into several bins as a function of its magnitude. Minimum and maximum thresholds define the range of motion (i.e. the range of amplitudes) to be processed. In one method, each bin contains equal ranges of amplitude [28,29]. Use of an amplitude-based method means that the various bins are unlikely to contain the same number of coincidences (Fig. 2c). Indeed, the number of statistics in a steep part of the RS will be lower than that in the end-expiratory phase. To overcome this issue, variable bin processing has been suggested; each bin contains the same statistics but with variable remaining motion amplitude [28].

Fig. 2

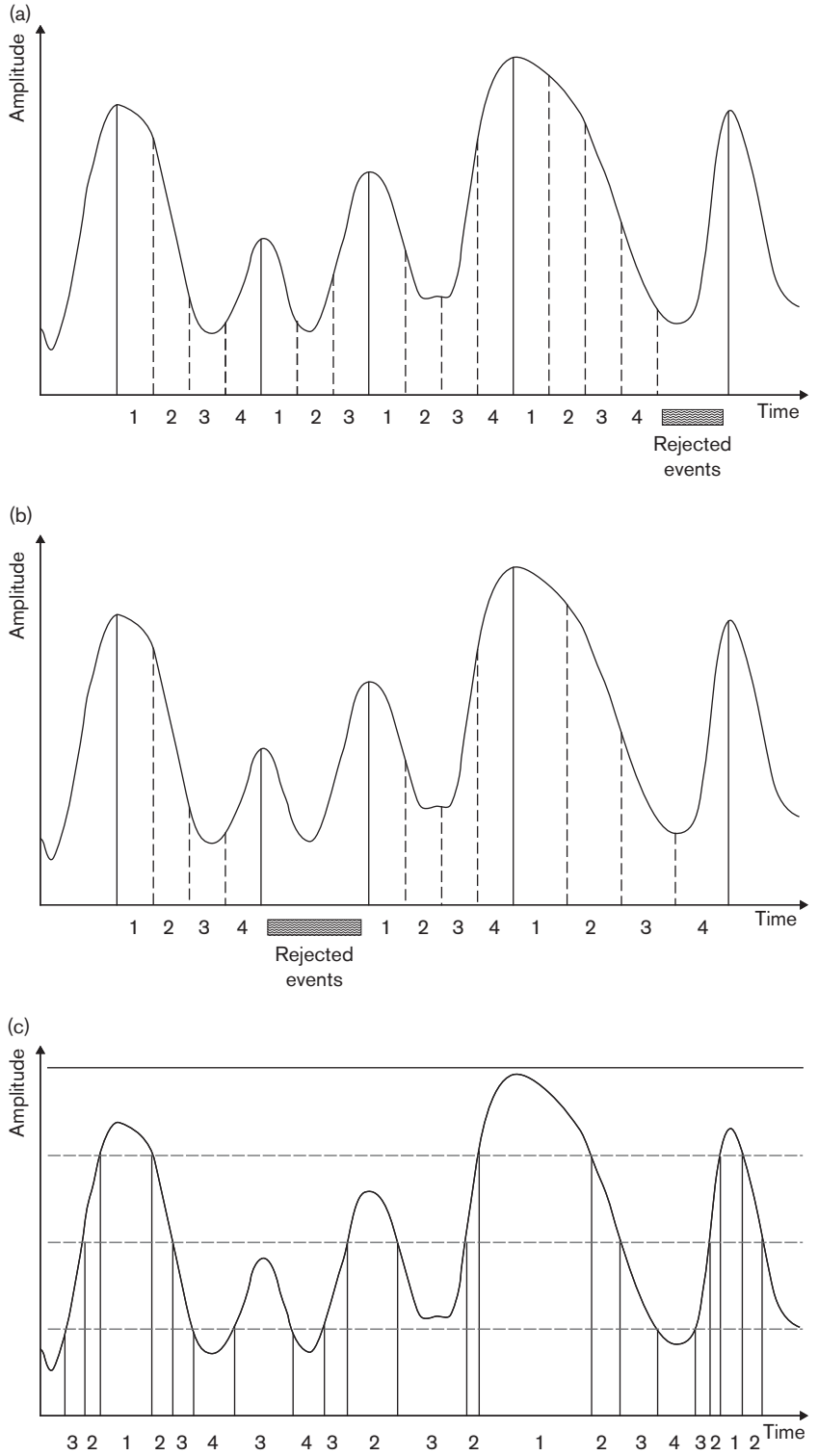

Four different gating schemes: (a) a time-based scheme, setting a fixed time for all bins throughout each respiratory cycle; (b) a time-based scheme, with division into the same number of bins for each respiratory cycle; (c) an amplitude-based scheme with equal-sized bins.

Table 1 Overview of studies using time-based methods

	Werner *et al.* [24]	Lupi *et al.* [25]		García Vicente *et al.* [26]		Kasuya *et al.* [27]	
Gating							
Tracking device	RPM	RPM		RPM		AZ-733V	
Number of bins	8	6		6		5	
Lesions							
Site	Lung	UL	LL	UL	LL	Pancreatic head	Pancreatic groove
N	18	19	3	29	13	13	2
SUV_{max}							
Gated	11.8 (±5.5)	15.7 (±13.3)	10.1 (±10.9)	2.2 (±0.8)	2.5 (±0.9)	5.8 (±4.3)	
Ungated	9.2 (±4.8)	9.6 (±7.1)	5.9 (±6.0)	1.3 (±0.6)	1.4 (±0.4)	5.4 (±3.9)	

LL, lower lung; RPM, Real-Time Position Management system; SUV_{max}, maximum standardized uptake value; UL, upper lung.

As for the time-based methods, the number of bins is an important determinant of image quality. Dawood *et al.* [31] showed that the optimal configuration contained eight respiratory bins. However, Bettinardi *et al.* [35] emphasized that the number of gates needed is related to a lesion's size and displacement.

Although the amplitude-based approach is superior to the time-based approach [28,29], the workstations require access to the RS during data processing. Multibin approaches can describe a lesion's displacement during the RC, which can be of value for radiotherapy planning [36]. However, these two approaches do not provide adequate attenuation correction. Indeed, CT images, usually acquired in free-breathing mode in a single volume, show a number of respiratory artifacts and, furthermore, do not correspond to a defined respiratory state. These two phenomena introduce errors into the attenuation correction and quantification of the uptake [29].

Single-bin methods

The deep-inspiration breath-hold method

Nehmeh *et al.* [37] and Meirelles *et al.* [38] developed the deep-inspiration breath-hold (DIBH) method. A device is used to track RS and deliver voice instructions (e.g. 'breathe in', 'hold', and 'relax'). A 15-s CT scan chest is acquired while the patient holds his/her breath in deep end-inspiration. The PET stage consists of nine independent, 20-s breath-hold acquisitions (again during deep end-inspiration). The patient is allowed to relax for 20 s between each acquisition. Finally, these acquisitions are summed, corrected for attenuation (using the CT data), and reconstructed with a conventional algorithm (Fig. 3).

With the DIBH method, both PET and CT data are acquired at the same tissue position during a deep end-inspiration breath-hold; this guarantees accurate attenuation correction. However, repeated 20-s acquisitions may be stressful and tiring in dyspneic patients. Even when breathing is coached and monitored, there is no guarantee that the patient will hold his/her breath at the same point in all the acquisitions. To avoid the need for repeated breath-hold acquisition, two groups have shown that it is feasible to acquire PET data during a single DIBH [39–41]. Kawano *et al.* [39] and Torizuka *et al.* [41] respectively considered that a breath-hold of 30 or 20 s is sufficient. However, the body phantom studies used in these two studies do not fully model clinical reality because of high concentration of activity in the spheres and the absence of noise in the thoracic cavity.

The DIBH method has been assessed in routine clinical practice (mainly for lung imaging) [38–43]. Indeed, the method allows the fully expanded lungs to be imaged and small tumors can be detected easily. Other researchers have evaluated this method for imaging the abdomen [43,44]. The main findings of these DIBH studies are summarized in Table 2.

The computed tomography-based method

Daouk *et al.* [45] and Fin *et al.* [46] have described a CT-based method, in which a 10-min LM PET acquisition is performed. The patients then hold their breath at the normal end-expiration point for 6 s, during which a breath-hold CT (BH-CT) scan is performed. The RS is recorded throughout the two sessions. The researchers chose this normal end-expiration because it is the most reproducible phase of the RC [47]. Given that end-expiration lasts longer than any other phase, selecting the events recorded during this phase improves counting statistics and provides the best image quality. In end-expiration, a plateau on the RS corresponds to a specific tissue position. An event selection range (ESR) is defined around this plateau. The portions of the RS falling within this ESR thus define the portions of the LM that should be conserved. The selected PET data are attenuation-corrected with the BH-CT data during reconstruction. Placing the ESR around the breath-hold position defined by BH-CT acquisition provides accurate matching between anatomical and functional images and yields accurate attenuation correction (Fig. 4).

The drawback of using end-expiration is the low lung volume in this phase of the RC, which may make it more difficult to detect small tumors. Furthermore, the CT-based method rejects a large proportion of the acquired PET data. Hence, a 10-min acquisition is needed to achieve the same quality as a standard 3-min acquisition [48].

Fig. 3

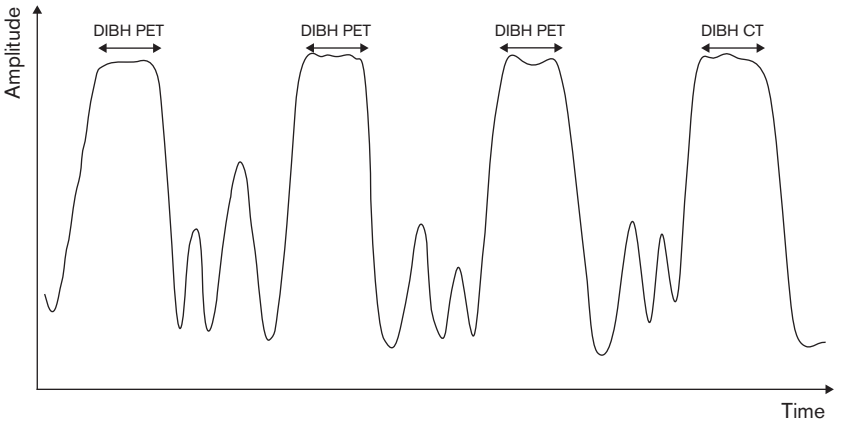

DIBH method: only PET data acquired during the patient's DIBH is retained for image reconstruction. CT, computed tomography; DIBH, deep-inspiration breath-hold.

Table 2 Overview of studies using the deep-inspiration breath-hold method

	Meirelles *et al.* [38]	Kawano *et al.* [39]		Kawano *et al.* [40]		Torizuka *et al.* [41]		Daisaki *et al.* [42]	Nagamachi *et al.* [43]		Nagamachi *et al.* [44]	
Protocol												
Number of breath-holds	9	1		1		1		>2	4		4	
Time (s)	180	30–125		30–143		20		120	120		120	
Lesions												
Site	Lung	UL	LL	UL	LL	UL	LL	Lung	Esophagus, chest, lung	Liver, bile duct, pancreas	Liver	Pancreas
N	62	78	30	40	55	22	25	32	NA	NA	NA	NA
Diameter (mm)	2–96[a]	12–40[a]	11–40[a]	16–60[a]	6–72[a]	28.8 (±14.8)	36.3 (±15.5)	25.9 (±6.9)	11.7 (±8.5)			
SUV_{max}												
Gated	8.0 (NA)	10.5 (±6.2)	7.8 (±3.9)	9.4 (±5.3)	10.6 (±4.9)	8.6 (±4.8)	13.6 (±8.3)	4.1 (±3.1)	12.0 (±8.9)	13.5 (±7.3)	18.4 (±4.2)	6.9 (±1.5)
Ungated	7.3 (NA)	9.1 (±5.5)	5.3 (±2.7)	7.5 (±4.7)	6.8 (±3.6)	7.0 (±3.9)	9.3 (±4.9)	4.3 (±2.8)	9.1 (±7.5)	9.5 (±4.4)	11.6 (±3.0)	6.0 (±1.3)

LL, lower lung; NA, not available; SUV_{max}, maximum standardized uptake value; UL, upper lung.
[a]Data provided with the range of results.

When applied to the lungs [46,49] and the liver [50,51], the CT-based method was found to be more sensitive than ungated imaging. Table 3 summarizes the differences in maximum standardized uptake values in these studies.

Chang *et al.* [52] have proposed a solution in which respiratory motion amplitude is captured during a whole-body CT acquisition. The RS amplitude is picked up at the entry and exit of the bed step where the lesion is localized in order to define an amplitude range (AR). Unlike the previously mentioned method, a gated, triggered LM acquisition then gathers only PET events corresponding to the defined AR. These PET data are used to generate a single motion-free volume. The drawback of this solution relates to its dependence on the patient's breathing pattern; if the patient breathes quickly, the influence of respiratory motion cannot be fully excluded. Moreover, the patient may not breathe in the same way for the CT and PET acquisitions. In such an event, the AR determined in the CT scan will not correspond to the respiratory amplitudes at the lesion's site according to the PET acquisition.

Data-driven approach

Nehmeh *et al.* [53] developed a gating method using a single tissue position. The tissue position is determined with respect to an external ^{18}F-FDG point source that appears on each image of a dynamic PET acquisition. On the first reconstructed frame, the point source's position is defined as the reference, and a region of interest (ROI) is drawn around it. The ROI is then carried over onto all frames but only those in which the point source falls within the ROI are considered. Finally, the corresponding PET raw data are summed and reconstructed.

Fig. 4

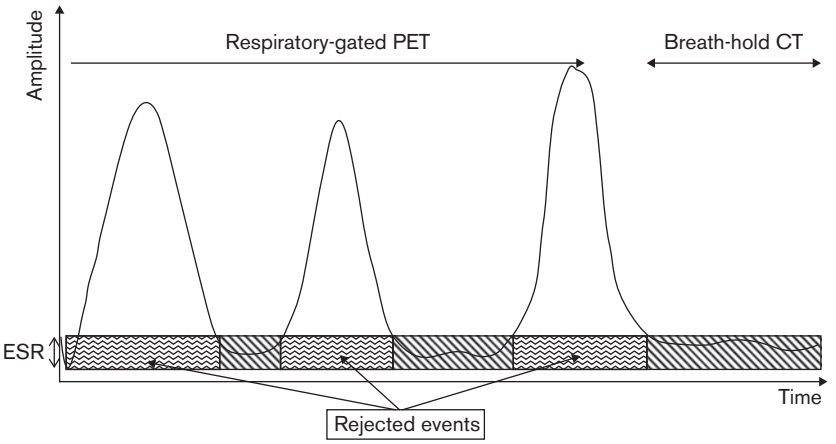

The CT-based method: the respiratory signal during breath-hold CT indicates the tissue position and is then used to define the ESR. CT, computed tomography; ESR, event selection range.

Table 3 Overview of studies using the computed tomography-based method

	Fin *et al.* [46]		Daouk *et al.* [49]		Daouk *et al.* [50]	Fin *et al.* [51]	
Lesions							
Site	UL	LL	Lung		Liver	Liver	
N	5	8	48		74	4	27
Diameter (mm)	14.0 (±5.3)		≤ 15	>15	15–25	10–14	≥ 15
SUV_{max}							
Gated	4.9 (±2.8)		2.3 (±1.8)	5.7 (±2.5)	8.5 (±3.5)	5.3 (±0.9)	7.7 (±3.2)
Ungated	3.8 (±2.3)		1.9 (±1.3)	5.2 (±2.5)	7.6 (±3.1)	4.8 (±0.5)	7.1 (±2.5)

LL, lower lung; SUV_{max}, maximum standardized uptake value; UL, upper lung.

Correction techniques

To avoid increasing the duration of PET acquisitions (due to the loss of statistics related to compensation techniques), some researchers have developed techniques to correct for respiratory motion. To the best of our knowledge, these techniques have not yet been used in routine clinical practice. Motion correction is usually performed by introducing a deformation field before, during, or after the tomographic reconstruction. Determination of the deformation field is beyond the scope of this paper but we shall detail these three approaches (before, during, or after reconstruction) in the following sections.

Prereconstruction correction methods: data-driven approaches

Prereconstruction correction involves changing the position of lines of response (LORs) [54–57] as a function of a precomputed deformation field. However, the LORs are displaced by means of affine transformations only; this means that the technique is well suited to the correction of head motion [58,59] but not to the correction of the nonrigid motion typically seen during breathing. The loss of some LORs may occur during repositioning (e.g. outside the gantry or between the detectors in 3D acquisitions) [57]. Moreover, the exact projection of the deformation field in raw space data may require a rounding step in LOR repositioning, which introduced noise into the final raw data [56].

Motion correction during reconstruction

With the availability of fast computers, PET images are usually obtained by applying expectation maximization algorithms [60–63]. Continuous-object reconstructions are generally based on discrete-data formulations through parallelepiped functions (i.e. voxels) and a system matrix, which links acquired data and the object's basis functions.

To correct for respiration motion, several groups have suggested the computation of a system matrix for each respiratory state [64–67]. The main drawback of these approaches relates to the rigid nature of the basis function commonly used. Indeed, voxels do not deform along with the motion correction, which generates discontinuities between voxels. The solution presented by Reyes and colleagues [68,69] uses spherical basis functions inscribed in voxels. Basis functions could be approximated by deformable ellipsoids, which avoid the discontinuities caused by tissue deformation.

Another way of correcting for respiratory motion is to take account of a-priori knowledge about an object (edges, anatomical features, etc.) by incorporating spatiotemporal

regularization into the reconstruction algorithm [70–74]. Grotus *et al.* [75] integrated temporal regularization with a temporally adaptive basis function. However, one drawback of these solutions relates to the determination of scalar weighting parameters, which can be performed empirically on phantoms but is not necessarily suited to clinical situations.

Postreconstruction motion correction

This method relies on summing gated images (obtained with a multibin approach) after a registration step [76–81]. In principle, this is an attractive approach, although PET image registration is complicated by the spatial resolution and by partial volume effects. In addition, this method suffers from the limitations described above in the section on multibin compensation. Moreover, the summed image is affected by the sum of the noise levels in each image. Nevertheless, registration of the gated PET images enables the determination of the deformation field required by the above-mentioned motion correction methods.

Future trends and conclusion

At the outset, respiratory motion compensation and correction techniques were aimed at improving diagnosis and follow-up during nuclear medicine examinations of the thorax and abdomen. However, recent advances in radiotherapy mean that metabolic images are taken into account in treatment planning [82]. Moreover, intensity-modulated radiotherapy planning and dose painting require information on the respiratory motion of lesions. In this context, multibin compensation techniques are the only methods capable of describing the lesion's path during the RC. Nevertheless, specific attenuation maps for each phase are required to describe intrinsic heterogeneities within lesions. One solution is provided by 4D CT, albeit at the cost of a substantial increase in the radiation dose and acquisition time. Now that combined PET/MRI scanners are becoming more widely available, a few reports have emphasized the value of MRI for correct PET images for respiratory motion [83–85]. In MRI, the patient is not exposed to ionizing radiation. Moreover, the fact that most recent gantries perform PET and MRI acquisitions simultaneously (rather than sequentially, as in PET/CT scanners) improves the quality of registration.

Acknowledgements

This work was funded by the Canceropôle Nord Ouest France.

The authors thank Dr David Fraser (Biotech Communication, Damery, France) for his helpful advice on the English language in this paper.

Conflicts of interest

There are no conflicts of interest.

References

1 Avril NE, Weber WA. Monitoring response to treatment in patients utilizing PET. *Radiol Clin North Am* 2005; **43**:189–204.
2 Fletcher JW, Djulbegovic B, Soares HP, Siegel BA, Lowe VJ, Lyman GH, *et al.* Recommendations on the use of ^{18}F-FDG PET in oncology. *J Nucl Med* 2008; **49**:480–508.
3 Gholamrezanezhad A, Chirindel A, Subramaniam R. Assessment of response to therapy. In: Peller P, Subramaniam R, Guermazi A, editors. *PET-CT and PET-MRI in oncology*. Berlin: Springer-Verlag; 2012. pp. 279–317.
4 Lardinois D, Weder W, Hany TF, Kamel EM, Korom S, Seifert B, *et al.* Staging of non-small-cell lung cancer with integrated positron-emission tomography and computed tomography. *N Engl J Med* 2003; **348**: 2500–2507.
5 Selzner M, Hany TF, Wildbrett P, McCormack L, Kadry Z, Clavien P-A. Does the novel PET/CT imaging modality impact on the treatment of patients with metastatic colorectal cancer of the liver? *Ann Surg* 2004; **240**:1027–1036.
6 Wade OL. Movements of the thoracic cage and diaphragm in respiration. *J Physiol* 1954; **124**:193–212.
7 Weiss PH, Baker JM, Potchen EJ. Assessment of hepatic respiratory excursion. *J Nucl Med* 1972; **13**:758–759.
8 Rodarte JR, Hubmayr RD, Stamenovic D, Walters BJ. Regional lung strain in dogs during deflation from total lung capacity. *J Appl Physiol* 1985; **58**:164–172.
9 Loring SH. Structural model of thorax and abdomen for respiratory mechanics. *Math Model* 1986; **7**:1083–1098.
10 Hubmayr RD, Rodarte JR, Walters BJ, Tonelli FM. Regional ventilation during spontaneous breathing and mechanical ventilation in dogs. *J Appl Physiol* 1987; **63**:2467–2475.
11 Osman MM, Cohade C, Nakamoto Y, Wahl RL. Respiratory motion artifacts on PET emission images obtained using CT attenuation correction on PET-CT. *Eur J Nucl Med Mol Imaging* 2003; **30**:603–606.
12 Fayad H, Pan T, Clement JF, Visvikis D. Technical note: correlation of respiratory motion between external patient surface and internal anatomical landmarks. *Med Phys* 2011; **38**:3157–3164.
13 Gierga DP, Brewer J, Sharp GC, Betke M, Willett CG, Chen GT. The correlation between internal and external markers for abdominal tumors: implications for respiratory gating. *Int J Radiat Oncol Biol Phys* 2005; **61**:1551–1558.
14 Koch N, Liu HH, Starkschall G, Jacobson M, Forster K, Liao Z, *et al.* Evaluation of internal lung motion for respiratory-gated radiotherapy using MRI: part I – correlating internal lung motion with skin fiducial motion. *Int J Radiat Oncol Biol Phys* 2004; **60**:1459–1472.
15 Nehmeh SA, Erdi YE, Pan T, Yorke E, Mageras GS, Rosenzweig KE, *et al.* Quantitation of respiratory motion during 4D-PET/CT acquisition. *Med Phys* 2004; **31**:1333–1338.
16 Riedel M. Respiratory motion estimation: tests and comparison of different sensors. Interdisciplinary Project. Technische Universität München Fakultät für Informatik, Germany; 2006.
17 Zhang T, Keller H, O'Brien MJ, Mackie TR, Paliwal B. Application of the spirometer in respiratory gated radiotherapy. *Med Phys* 2003; **30**: 3165–3171.
18 Otani Y, Fukuda I, Tsukamoto N, Kumazaki Y, Sekine H, Imabayashi E, *et al.* A comparison of the respiratory signals acquired by different respiratory monitoring systems used in respiratory gated radiotherapy. *Med Phys* 2010; **37**:6178–6186.
19 Boucher L, Rodrigue S, Lecomte R, Benard F. Respiratory gating for 3-dimensional PET of the thorax: feasibility and initial results. *J Nucl Med* 2004; **45**:214–219.
20 Didierlaurent D, Ribes S, Caselles O, Jaudet C, Cazalet JM, Batatia H, *et al.* A new respiratory gating device to improve 4D PET/CT. *Med Phys* 2013; **40**:032501.
21 Bruyant PP, Cheze Le Rest C, Turzo A, Jarritt P, Carson K, Visvikis D. A method for synchronizing an external respiratory signal with a list-mode PET acquisition. *Med Phys* 2007; **34**:4472–4475.
22 Nehmeh SA, Erdi YE, Ling CC, Rosenzweig KE, Schoder H, Larson SM, *et al.* Effect of respiratory gating on quantifying PET images of lung cancer. *J Nucl Med* 2002; **43**:876–881.
23 Nehmeh SA, Erdi YE, Ling CC, Rosenzweig KE, Squire OD, Braban LE, *et al.* Effect of respiratory gating on reducing lung motion artifacts in PET imaging of lung cancer. *Med Phys* 2002; **29**:366–371.
24 Werner MK, Parker JA, Kolodny GM, English JR, Palmer MR. Respiratory gating enhances imaging of pulmonary nodules and measurement of tracer uptake in FDG PET/CT. *Am J Roentgenol* 2009; **193**:1640–1645.
25 Lupi A, Zaroccolo M, Salgarello M, Malfatti V, Zanco P. The effect of ^{18}F-FDG-PET/CT respiratory gating on detected metabolic activity in lung lesions. *Ann Nucl Med* 2009; **23**:191–196.

26 Garcia Vicente AM, Soriano Castrejon AM, Talavera Rubio MP, Leon Martin AA, Palomar Munoz AM, Pilkington Woll JP, *et al*. (18)F-FDG PET-CT respiratory gating in characterization of pulmonary lesions: approximation towards clinical indications. *Ann Nucl Med* 2010; **24**:207–214.

27 Kasuya T, Tateishi U, Suzuki K, Daisaki H, Nishiyama Y, Hata M, *et al*. Role of respiratory-gated PET/CT for pancreatic tumors: a preliminary result. *Eur J Radiol* 2012; **82**:69–74.

28 Dawood M, Buther F, Lang N, Schober O, Schafers KP. Respiratory gating in positron emission tomography: a quantitative comparison of different gating schemes. *Med Phys* 2007; **34**:3067–3076.

29 Daouk J, Fin L, Bailly P, Meyer ME. Respiratory-gated positron emission tomography and breath-hold computed tomography coupling to reduce the influence of respiratory motion: methodology and feasibility. *Acta Radiol* 2009; **50**:144–155.

30 Vauclin S, Hapdey S, Michel C, Rebani H, Buvat I, Edet-Sanson A, *et al*. Monte Carlo simulations of respiratory gated ^{18}F-FDG PET for the assessment of volume measurement methods. Nuclear Science Symposium Conference Record, 2008 IEEE; 19–25 October, Dresden, Germany; 2008. pp. 4050–4053.

31 Dawood M, Buther F, Stegger L, Jiang X, Schober O, Schafers M, *et al*. Optimal number of respiratory gates in positron emission tomography: a cardiac patient study. *Med Phys* 2009; **36**:1775–1784.

32 Teo BK, Saboury B, Munbodh R, Scheuermann J, Torigian DA, Zaidi H, *et al*. The effect of breathing irregularities on quantitative accuracy of respiratory gated PET/CT. *Med Phys* 2012; **39**:7390–7397.

33 Hoffman EJ, Huang SC, Plummer D, Phelps ME. Quantitation in positron emission computed tomography: 6. Effect of nonuniform resolution. *J Comput Assist Tomogr* 1982; **6**:987–999.

34 Alessio AM, Kinahan PE. Improved quantitation for PET/CT image reconstruction with system modeling and anatomical priors. *Med Phys* 2006; **33**:4095–4103.

35 Bettinardi V, Rapisarda E, Gilardi MC. Number of partitions (gates) needed to obtain motion-free images in a respiratory gated 4D-PET/CT study as a function of the lesion size and motion displacement. *Med Phys* 2009; **36**:5547–5558.

36 Bowen SR, Nyflot MJ, Gensheimer M, Hendrickson KR, Kinahan PE, Sandison GA, *et al*. Challenges and opportunities in patient-specific, motion-managed and PET/CT-guided radiation therapy of lung cancer: review and perspective. *Clin Transl Med* 2012; **1**:1–18.

37 Nehmeh SA, Erdi YE, Meirelles GS, Squire O, Larson SM, Humm JL, *et al*. Deep-inspiration breath-hold PET/CT of the thorax. *J Nucl Med* 2007; **48**:22–26.

38 Meirelles GS, Erdi YE, Nehmeh SA, Squire OD, Larson SM, Humm JL, *et al*. Deep-inspiration breath-hold PET/CT: clinical findings with a new technique for detection and characterization of thoracic lesions. *J Nucl Med* 2007; **48**:712–719.

39 Kawano T, Ohtake E, Inoue T. Deep-inspiration breath-hold PET/CT of lung cancer: maximum standardized uptake value analysis of 108 patients. *J Nucl Med* 2008; **49**:1223–1231.

40 Kawano T, Ohtake E, Inoue T. Deep-inspiration breath-hold PET/CT versus free breathing PET/CT and respiratory gating PET for reference: evaluation in 95 patients with lung cancer. *Ann Nucl Med* 2011; **25**:109–116.

41 Torizuka T, Tanizaki Y, Kanno T, Futatsubashi M, Yoshikawa E, Okada H, *et al*. Single 20-s acquisition of deep-inspiration breath-hold PET/CT: clinical feasibility for lung cancer. *J Nucl Med* 2009; **50**:1579–1584.

42 Daisaki H, Shinohara H, Terauchi T, Murano T, Shimada N, Moriyama N, *et al*. Multi-bed-position acquisition technique for deep inspiration breath-hold PET/CT: a preliminary result for pulmonary lesions. *Ann Nucl Med* 2010; **24**:179–188.

43 Nagamachi S, Wakamatsu H, Kiyohara S, Fujita S, Futami S, Arita H, *et al*. The reproducibility of deep-inspiration breath-hold (18)F-FDG PET/CT technique in diagnosing various cancers affected by respiratory motion. *Ann Nucl Med* 2010; **24**:171–178.

44 Nagamachi S, Wakamatsu H, Kiyohara S, Fujita S, Futami S, Arita H, *et al*. Usefulness of a deep-inspiration breath-hold ^{18}F-FDG PET/CT technique in diagnosing liver, bile duct, and pancreas tumors. *Nucl Med Commun* 2009; **30**:326–332.

45 Daouk J, Fin L, Bailly P, Meyer ME. Improved attenuation correction via appropriate selection of respiratory-correlated PET data. *Comput Methods Programs Biomed* 2008; **92**:90–98.

46 Fin L, Daouk J, Morvan J, Bailly P, El Esper I, Saidi L, *et al*. Initial clinical results for breath-hold CT-based processing of respiratory-gated PET acquisitions. *Eur J Nucl Med Mol Imaging* 2008; **35**:1971–1980.

47 Van Elmpt W, Hamill J, Jones J, De Ruysscher D, Lambin P, Ollers M. Optimal gating compared to 3D and 4D PET reconstruction for characterization of lung tumours. *Eur J Nucl Med Mol Imaging* 2011; **38**:843–855.

48 Daouk J, Fin L, Bailly P, Meyer M-E. AW-OSEM parameter optimization for selected events related to the breath-hold CT position in respiratory-gated PET acquisition. Fifth IEEE International Symposium on Biomedical Imaging; 14–17 May, Paris, France; 2008. pp. 1323–1326.

49 Daouk J, Leloire M, Fin L, Bailly P, Morvan J, El Esper I, *et al*. Respiratory-gated ^{18}F-FDG PET imaging in lung cancer: effects on sensitivity and specificity. *Acta Radiol* 2011; **52**:651–657.

50 Daouk J, Fin L, Bailly P, Slama J, Diouf M, Morvan J, *et al*. The benefits of respiratory gating in ^{18}F-FDG PET imaging of the liver. *IJNESE* 2012; **2**:5–10.

51 Fin L, Daouk J, Bailly P, Slama J, Morvan J, El Esper I, *et al*. Improved imaging of intrahepatic colorectal metastases with ^{18}F-fluorodeoxyglucose respiratory-gated positron emission tomography. *Nucl Med Commun* 2012; **33**:656–662.

52 Chang G, Chang T, Pan T, Clark JW Jr, Mawlawi OR. Implementation of an automated respiratory amplitude gating technique for PET/CT: clinical evaluation. *J Nucl Med* 2010; **51**:16–24.

53 Nehmeh SA, Erdi YE, Rosenzweig KE, Schoder H, Larson SM, Squire OD, *et al*. Reduction of respiratory motion artifacts in PET imaging of lung cancer by respiratory correlated dynamic PET: methodology and comparison with respiratory gated PET. *J Nucl Med* 2003; **44**:1644–1648.

54 Chung AJ, Camici PG, Yang G-Z. List-mode affine rebinning for respiratory motion correction in PET cardiac imaging. In: Yang G-Z, editor. *International Workshop on Medical Image and Augmented Reality, Shanghai*. Berlin, Heidelberg: Springer-Verlag; 2006. pp. 293–300.

55 Lamare F, Cresson T, Savean J, Cheze Le Rest C, Reader AJ, Visvikis D. Respiratory motion correction for PET oncology applications using affine transformation of list mode data. *Phys Med Biol* 2007; **52**:121–140.

56 Livieratos L, Stegger L, Bloomfield PM, Schafers K, Bailey DL, Camici PG. Rigid-body transformation of list-mode projection data for respiratory motion correction in cardiac PET. *Phys Med Biol* 2005; **50**:3313–3322.

57 Rahmim A, Bloomfield P, Houle S, Lenox M, Michel C, Buckley KR, *et al*. Motion compensation in histogram-mode and list-mode EM reconstructions: beyond the event-driven approach. *IEEE Trans Nucl Sci* 2004; **51**: 2588–2596.

58 Fulton R, Nickel I, Tellmann L, Meikle S, Pietrzyk U, Herzog H. Event-by-event motion compensation in 3D PET. Nuclear Science Symposium Conference Record; 2003 IEEE, 19–25 October, Portland, Oregon, USA; 2003. pp. 3286–3289.

59 Thielemans K, Mustafovic S, Schnorr L. Image reconstruction of motion corrected sonograms. Nuclear Science Symposium Conference Record, 2003 IEEE; 19–25 October, Portland, Oregon, USA; 2003. pp. 2401–2406.

60 Comtat C, Kinahan PE, Defrise M, Michel C, Townsend DW. Fast reconstruction of 3D PET data with accurate statistical modeling. *IEEE Trans Nucl Sci* 1998; **45**:1083–1089.

61 Green PJ. Bayesian reconstructions from emission tomography data using a modified EM algorithm. *IEEE Trans Med Imaging* 1990; **9**:84–93.

62 Hudson H, Larkin R. Accelerated image reconstruction using ordered subsets of projection data. *IEEE Trans Med Imaging* 1994; **13**:601–609.

63 Shepp L, Vardi Y. Maximum likelihood reconstruction for emission tomography. *IEEE Trans Med Imaging* 1982; **1**:113–122.

64 Fin L, Bailly P, Daouk J, Meyer ME. Motion correction based on an appropriate system matrix for statistical reconstruction of respiratory-correlated PET acquisitions. *Comput Methods Programs Biomed* 2009; **96**:e1–e9.

65 Lamare F, Ledesma Carbayo MJ, Cresson T, Kontaxakis G, Santos A, Le Rest CC, *et al*. List-mode-based reconstruction for respiratory motion correction in PET using non-rigid body transformations. *Phys Med Biol* 2007; **52**:5187–5204.

66 Li T, Thorndyke B, Schreibmann E, Yang Y, Xing L. Model-based image reconstruction for four-dimensional PET. *Med Phys* 2006; **33**:1288–1298.

67 Qiao F, Pan T, Clark JW Jr, Mawlawi OR. A motion-incorporated reconstruction method for gated PET studies. *Phys Med Biol* 2006; **51**:3769–3783.

68 Reyes M, Malandain G, Koulibaly PM, Gonzalez Ballester MA, Darcourt J. Respiratory motion correction in emission tomography image reconstruction. *Med Image Comput Comput Assist Interv* 2005; **8**:369–376.

69 Reyes M, Malandain G, Koulibaly PM, Gonzalez-Ballester MA, Darcourt J. Model-based respiratory motion compensation for emission tomography image reconstruction. *Phys Med Biol* 2007; **52**:3579–3600.

70 Blume M, Martinez-Moller A, Keil A, Navab N, Rafecas M. Joint reconstruction of image and motion in gated positron emission tomography. *IEEE Trans Med Imaging* 2010; **29**:1892–1906.

71 Cao Z, Gilland DR, Mair BA, Jaszczak RJ. Three-dimensional motion estimation with image reconstruction for gated cardiac ECT. *IEEE Trans Nucl Sci* 2003; **50**:384–388.

72 Gravier EJ, Yongyi Y. Motion-compensated reconstruction of tomographic image sequences. *IEEE Trans Nucl Sci* 2005; **52**:51–56.

73 Jacobson MW, Fessler JA. Joint estimation of image and deformation parameters in motion-corrected PET. Nuclear Science Symposium Conference Record, 2003 IEEE; 19–25 October, Portland, Oregon, USA; 2003. pp. 3290–3294.

74 Qiao F, Clark JW, Pan T, Mawlawi O. Joint model of motion and anatomy for PET image reconstruction. *Med Phys* 2007; **34**:4626–4639.

75 Grotus N, Reader AJ, Stute S, Rosenwald JC, Giraud P, Buvat I. Fully 4D list-mode reconstruction applied to respiratory-gated PET scans. *Phys Med Biol* 2009; **54**:1705–1721.

76 Bai W, Brady M. Regularized B-spline deformable registration for respiratory motion correction in PET images. *Phys Med Biol* 2009; **54**:2719–2736.

77 Dawood M, Buther F, Jiang X, Schafers KP. Respiratory motion correction in 3-D PET data with advanced optical flow algorithms. *IEEE Trans Med Imaging* 2008; **27**:1164–1175.

78 Dawood M, Lang N, Jiang X, Schafers KP. Lung motion correction on respiratory gated 3-D PET/CT images. *IEEE Trans Med Imaging* 2006; **25**:476–485.

79 Gao J, Chai P, Yun M-K, Liu S-Q, Bao-Ci S, Wei L. Respiratory motion correction with an improved demons algorithm for PET image. *Chinese Phys C* 2012; **36**:1025–1030.

80 Klein GJ, Reutter BW, Huesman RH. 4D affine registration models for respiratory-gated PET. Nuclear Science Symposium Conference Record, 2000 IEEE; 15–20 October, Lyon, France; 2000. pp. 15/41–15/45.

81 Schäfers KP, Dawood M, Lang N, Büther F, Schäfers M, Schober O. Motion correction in PET/CT. *Nuklearmedizin* 2005; **44**:46–50.

82 Sattler B, Lee JA, Lonsdale M, Coche E. PET/CT (and CT) instrumentation, image reconstruction and data transfer for radiotherapy planning. *Radiother Oncol* 2010; **96**:288–297.

83 Chun SY, Reese TG, Ouyang J, Guerin B, Catana C, Zhu X, *et al*. MRI-based nonrigid motion correction in simultaneous PET/MRI. *J Nucl Med* 2012; **53**:1284–1291.

84 Guerin B, Cho S, Chun SY, Zhu X, Alpert NM, El Fakhri G, *et al*. Nonrigid PET motion compensation in the lower abdomen using simultaneous tagged-MRI and PET imaging. *Med Phys* 2011; **38**:3025–3038.

85 Wurslin C, Schmidt H, Martirosian P, Brendle C, Boss A, Schwenzer NF, *et al*. Respiratory motion correction in oncologic PET using T1-weighted MR imaging on a simultaneous whole-body PET/MR system. *J Nucl Med* 2013; **54**:464–471.